JOURNAL OF MATERIALS SCIENCE 16 (1981) 1835–1842

Defects in polydiacetylene single crystals

Part 1 The perfect crystal and stacking faults

R. J. YOUNG, R. T. READ
Department of Materials, Queen Mary College, Mile End Road, London E1 4NS, UK
J. PETERMANN
Werkstoffphysik und Werkstofftechnologie, University of the Saarland, Bau 2, 6600 Saarbrücken, W. Germany

The structure of single crystals of a substituted polydiacetylene (pTS) has been investigated using transmission electron microscopy. The structure of the perfect crystal has been examined and it has been shown that the molecules lie in the plane of the lamellar crystals in an extended-chain conformation. The formations of bend contour zone axis patterns has been analysed and they are found to be due to the crystal being deformed into the shapes of both cups (or domes) and saddles. A common defect in the crystals was a stacking fault; using dark-field microscopy it has been found to have a displacement vector of $\frac{1}{2}[1\,\bar{2}\,1]$. It has been shown that such a stacking fault can be accommodated without any disruption to either the molecular backbone or the relatively large side-groups on the molecule. The significance of these stacking faults with regard to the structure of polymer crystals in general is discussed.

1. Introduction

All crystals of materials are known to contain defects such as dislocations, stacking faults and vacancies but knowledge of such defects in polymer crystals is somewhat limited. This is rather unfortunate because there are several reasons why interest should be shown in defects in macromolecular crystals, for example:

(a) From a fundamental view-point it is essential to know what types of defects exist in polymer crystals and how they compare with defects in crystals of other materials;

(b) It is desirable to know if there is any correlation between the presence of defects and the mechanical or electrical properties of polymer crystals.

The study of defects in metal crystals has been undertaken using electron microscopy for over 25 years and a high level of understanding of metal defects has now been reached. In contrast, relatively little is known about the types of defects that can exist in polymer crystals. There are two main reasons for this. The first is that single crystals of conventional polymers are normally in the form of microscopic chain-folded lamellae with the molecules orientated approximately perpendicular to the large crystal surface [1]. This lamellar morphology imposes limitations upon the orientations in which the crystals can be viewed.

The second reason is that conventional polymers tend to suffer radiation damage in the electron beam [2]. This means that the time available to study defects in any particular crystal is severely limited as the crystals rapidly become damaged by the radiation. In addition, defects can be induced by the radiation itself.

There has been some notable success in identifying dislocations in lamellar polyethylene single crystals: edge dislocations caused by the termination of fold-planes within the crystals have been identified using Moiré techniques [3], interfacial dislocations have been seen in overlapping single crystals [4] and screw dislocations with Burgers vectors parallel to the chain direction have been identified through their associated surface relaxations [5]. However, the chain-folded crystal morphology restricts investigations to viewing the

0022–2461/81/071835–08$02.80/0 © *1981 Chapman and Hall Ltd.*

crystals in the electron microscope parallel to the chain direction and defects which can only be observed by viewing crystals in directions perpendicular to the chain direction therefore cannot be investigated. This particular problem has now been overcome by the preparation of large, relatively perfect polymer single-crystals by solid-state polymerization [6]. This technique involves the growth of crystals of the monomer in the form of single crystal and the subsequent polymerization reaction takes place in the solid state [6]. Suitable monomers include sulphur nitride [7] and certain substituted diacetylenes [8]. Polymers from these monomers can be obtained in the form of good single crystals with the molecules in a chain-extended conformation. Previous investigations by the authors using transmission electron microscopy have shown that polymeric sulphur nitride $(SN)_x$ [9, 10] and polydiacetylenes [11, 12] can be obtained in the form of thin single-crystal films in which the molecules are extended in the plane of the film and its is the purpose of this series of papers to report new observations concerning defects in polydiacetylene single crystals. The defects are of interest from both a fundamental view-point and also because there have been suggestions that defects can affect the polymerization behaviour of diacetylene crystals [13].

The first paper is concerned with the structure of thin films of the polymer based upon the bis-(p-toluene sulphonate) ester of 2,4-hexadiyne–1,6-diol which will henceforth be referred to as pTS. Detailed investigations into the structure of the perfect crystal are described and the discovery of stacking faults within the crystals is reported. As far as the authors are aware, this is the first report of the direct observation of stacking faults in polymer crystals and, as such, has an important bearing upon the structure of polymer crystals in general. Subsequent papers will be concerned with the types of dislocations and dislocation arrays that are found in polydiacetylene crystals.

2. Experimental procedure

Monomer crystals prepared by conventional techniques, described elsewhere [8], were supplied by Dr D. Bloor and Mr D. Ando of Queen Mary College. The monomer was dissolved in xylene to give a solution of concentration approximately 0.001 M; the solution was filtered to remove any traces of polymer which were present as a suspension of fine red particles. The crystals to be used for the electron microscope studies were prepared by putting a few drops of monomer solution onto the surface of a bath of distilled water and allowing the xylene to evaporate. The process was sometimes accelerated by allowing the evaporation to take place in the air-flow of a fume cupboard. The monomer crystals, which formed on the surface of the water, were collected on 400-mesh electron microscope copper grids. The crystals were then polymerized by heating them on the grids in an oven for 20 h at 70° C [8]. The polymer crystals were subsequently examined in a JEOL 200A transmission electron microscope operated at an accelerating voltage of 200 kV. In order to minimize the amount of damage caused to the crystals by the electron beam they were viewed at low intensity levels and the micrographs were obtained using sensitive X-ray plates (Agfa D10).

3. Analysis of the perfect crystal

Although this particular paper is concerned principally with defects that are found in polydiacetylene single crystals it is essential that the structure of the perfect crystal should be understood before defects can be considered.

3.1. General crystal area

The main points of interest concerning the perfect crystal are the crystal structure of the polymer, the orientation of the molecules and the general crystal habit. Fig. 1a shows a bright-field electron micrograph of a typical defect-free area of a pTS crystal; Fig. 1b shows a corresponding dark-field electron micrograph of the same area imaged with the strong spot of the diffraction pattern (given in the insert). Since the crystal structure of pTS macrocrystals is known to be monoclinic ($P2_1/a$) with unit-cell dimensions of $a = 1.494$ nm, $b = 1.449$ nm, $c = 0.491$ nm and $\gamma = 118.1°$ [14, 15], it has been possible to confirm that the pTS crystals used in the present investigation have the same structure. Also, from the relative orientations of the diffraction patterns and the pTS crystals it has been possible to show that the polymer molecules lie in the plane of the crystals and that the crystals are lamellar with surfaces corresponding to (0 1 0) crystal planes [11].

The main feature of the bright-field electron micrographs of pTS crystals is the many bend contours that can be seen. If there is sufficient lattice distortion, the bend contours in the dark-field views may consist of a single band with

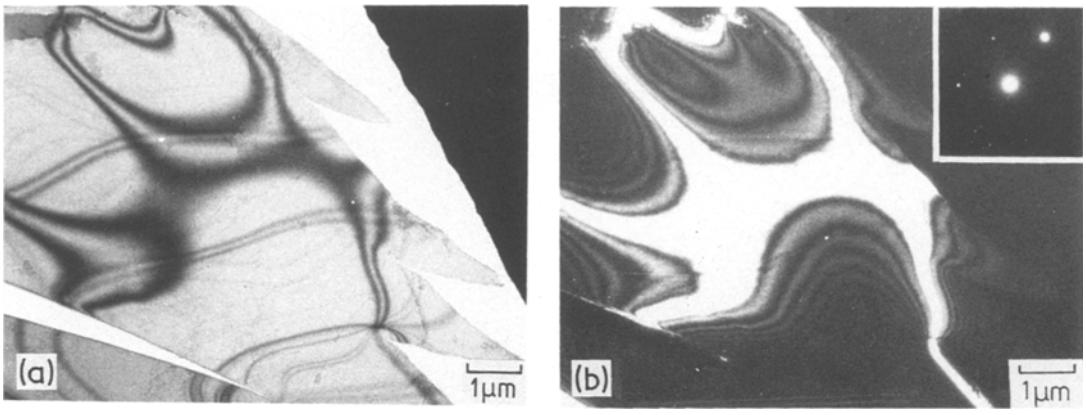

Figure 1 Electron micrographs of the same area of a thin film of pTS. (a) Bright-field micrograph; (b) dark-field micrograph using g = 2 $\bar{1}$ 1 (diffraction pattern in the insert).

several subsidiary lines. The appearance of the bend contours is similar of those found in thin foils of metals [15] and other materials [16] and the broadness of the bands is a measure of the amount of elastic bending of the particular lattice planes used for imaging. The formation and appearance of the contours can be explained in terms of the kinematical or dynamical theories of contrast for electron diffraction [17]. Generally speaking, the bright lines or areas in the dark-field micrographs are regions of exactly the same lattice orientation for a particular plane.

3.2. Bend-contour zone axis patterns

The presence of a bend contour indicates that the crystal in that region is diffracting in a particular Bragg diffraction condition [16, 17]. If the specimen is tilted in the electron microscope the bend contours move. Sometimes several bend contours can be seen to cross at a point and when this happens the Bragg diffraction conditions for several different lattice planes must be simultaneously satisfied; the crossing points are referred to as "bend-contour zone axis patterns". Figs 2 and 3 show examples of zone axis patterns in pTS crystals. Selected area diffraction patterns (SADP) are also given and in both cases they correspond to

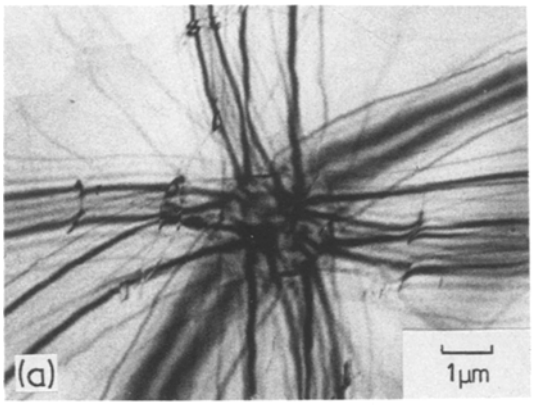

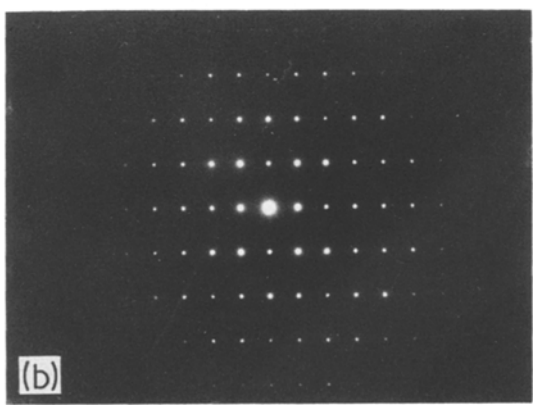

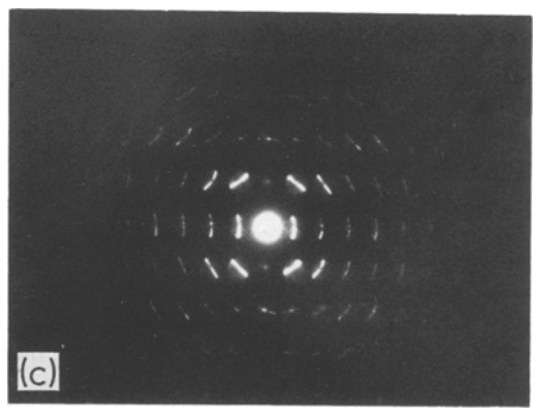

Figure 2 [1 2 0] zone axis in a pTS crystal. (a) Bright-field micrograph; (b) selected area diffraction pattern from the centre of the zone axis; (c) multiple dark-field SAD pattern taken of the same area as (b) obtained by defocussing the intermediate lens.

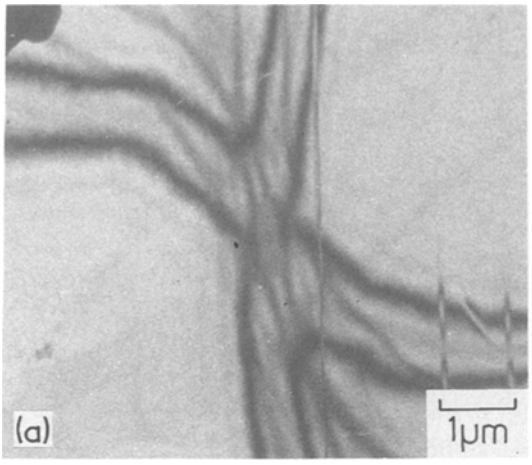

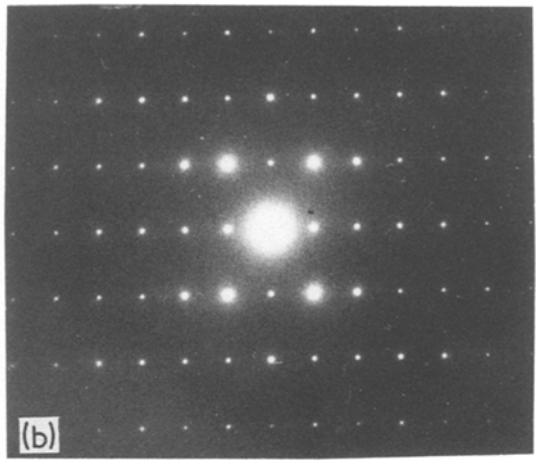

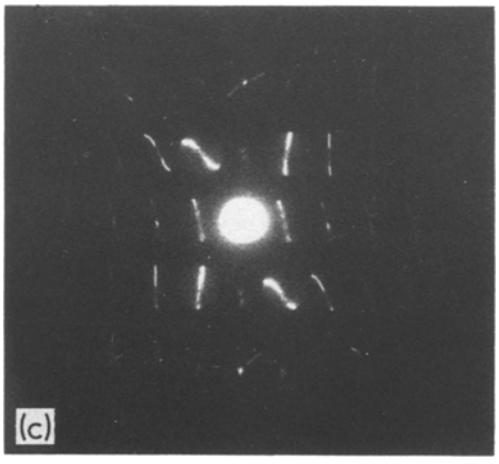

Figure 3 [1 2 0] zone axis in a pTS crystal. (a) Bright-field micrograph; (b) selected area diffraction pattern from the centre of the zone axis; (c) multiple dark-filed SAD pattern taken of the same area as (b).

a beam direction of [1 2 0], consistent with the incident beam being approximately perpendicular to the (0 1 0) face of the monoclinic [14, 15] crystals.

There has recently been considerable interest in analysing bend-contour zone axis patterns in metal foils [18, 19] and using the patterns to help with the identification of defects in molecular crystals [16]. It was generally thought that the patterns were formed where the crystal was elastically deformed into the cup- or dome-like shapes [18] but Shannon and Eades [19] have pointed out that this may not always be the case and that saddle points can produce similar patterns. They showed that saddle points could be differentiated from cups or domes by obtaining a multiple dark-field image of the specimen, achieved by obtaining a SADP and de-focussing the intermediate lens [19]. This procedure has been followed in Figs 2c and 3c and it can be seen that the micrographs consist of a series of low-magnification, low-resolution, dark-field images of the pole arranged in the same pattern as the SADP. The two possible arrangements of the contours in the multiple dark-field patterns for saddle points and for domes or cups are sketched in Fig. 4a and b, following Shannon and Eades [19]. Inspection of the two multiple dark-field patterns, Figs 2c and 3c, shows that the feature giving rise to the bend-contour zone axis pattern in Fig. 2 is a dome or cup and that in Fig. 3 is a saddle point. These characteristic patterns are found to be very common in thin pTS crystals and probably form when the crystals are buckled or distorted. It is likely that this will occur more readily in relatively low modulus polymer films than in higher modulus metal foils.

Jones and Thomas [16] have recently pointed out the usefulness of bend-contour zone axis patterns in the study of molecular crystals by

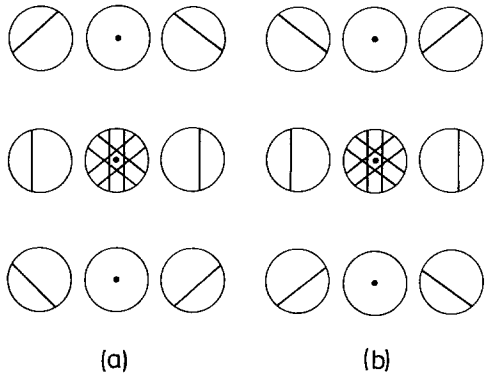

Figure 4 Expected arrangements of the bend contours in multiple dark-field patterns for [1 2 0] zone axis in pTS, following the analysis of Shannon and Eades [19].

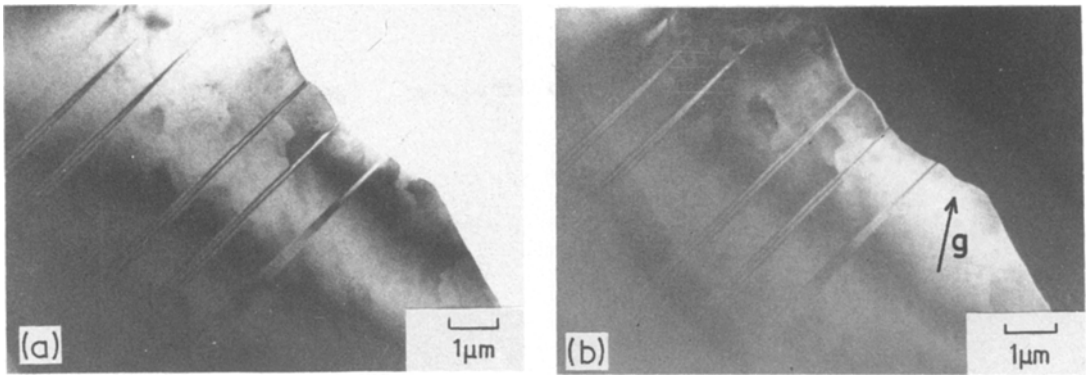

Figure 5 Stacking faults in a thick pTS crystal. (a) Bright-field electron micrograph; (b) dark-field electron micrograph obtained using $\mathbf{g} = 2\,\bar{1}\,1$.

electron microscopy, so-called "real-space crystallography". Although these materials are invariably beam-sensitive, they were able to show that the bend-contour zone axis patterns could be used to help in the indexing of reflections, interpretation of crystal structures and in the analysis of defects [16]. Beam damage often limits the time available to, for example, observe defects in different dark-field conditions but, from the way particular defects interact with the bend-contours around a zone axis, it is often possible to identify the defect without need to use the technique of dark-field electron microscopy [16].

The pTS crystals used in this present study did not appear to be particularly beam-sensitive, probably because of their conjugated back-bone [6]. Since they are sufficiently robust to allow a series of diffraction patterns and bright- and dark-field electron micrographs to be obtained from the same area before beam damage becomes significant, the defects which are described in the next section have been analysed using conventional dark-field techniques which lead to a more accurate and detailed analysis of defects than can be obtained using real-space crystallography.

4. Analysis of the stacking faults

Examination of the bright-field electron micrographs of the poles in Figs 2 and 3 shows that some of the bend contours are stepped or otherwise disturbed, indicating the presence of defects in the crystals. It is clear that there are several types of inherent defects which exist in pTS crystals and in this paper it will be shown that one type of defect commonly found is a stacking fault.

Fig. 5 shows a bright- and dark-field electron micrograph of a relatively thick wedge-shaped pTS crystal; both micrographs were obtained with imaging $\mathbf{g} = [2\,\bar{1}\,1]$. The main features that can be seen are five defects which lie parallel to the chain direction and become narrower as they approach the specimen edge. The defects each display characteristic black/white fringes and closer examination shows that the contrast is reversed between the dark- and bright-field images. The defects in Fig. 5 are very similar in appearance to stacking faults, such as those which are found in metals (compare with Fig. 10.11a in [17]). These are planar defects produced by a layer of incorrectly stacked atoms (in the case of metals) or molecules (in the case of molecular solids). The planar nature of the defects in Fig. 5 is apparent from the way in which they taper towards the edge of the crystal. This is due to the crystal being wedge-shaped and the planar defects lying on planes inclined at an oblique angle in the crystal.

The defects are also found to give either strong or weak contrast depending upon the **g** used to image them in the dark-field. This can be seen very clearly from Fig. 6 where the same defects give strong contrast for $\mathbf{g} = [2\,\bar{1}\,1]$ and $\mathbf{g} = [4\,\bar{2}\,1]$ but appear only weakly for $\mathbf{g} = [2\,\bar{1}\,0]$.

4.1. Identification of stacking faults

The contrast and diffraction observations upon the fringed linear defects can be summarized as follows:

(a) the defects remain stationary upon tilting the sample with respect to the electron beam (i.e. upon changing the s-condition);

(b) the number of fringes resolved depends upon the sample thickness (Fig. 5) and the s-condition (Fig. 6);

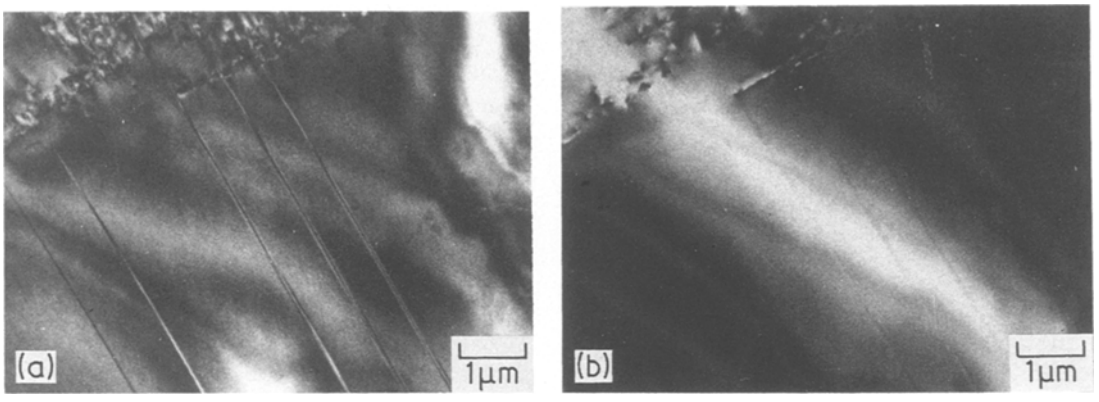

Figure 6 Dark-field electron micrographs of stacking faults in the same area of a thin crystal of pTS obtained using different imaging vectors: (a) $\mathbf{g} = 2\,\bar{1}\,1$, (b) $\mathbf{g} = 2\,\bar{1}\,0$ and (c) $\mathbf{g} = 4\,\bar{2}\,1$.

(c) the fringes seen in dark- and bright-fields are complementary (Fig. 5);

(d) the intensity of the fringes in the defect varies approximately as a $\cos^2$ function;

(e) the visibility of the defects depends upon the **g**-vector used for imaging (Fig. 6);

(f) the lattice orientation on both sides of the defects is identical;

(g) the defects terminate either at dislocations or at the specimen edge;

(h) the line of the defects is parallel to a crystallographic direction, c, which is the chain direction;

(i) selected area electron diffraction obtained from an area containing several defects gives single-crystal diffraction patterns and there is no change of lattice orientation within the defect.

Many of these observations are typical of those expected for an interface in the crystals such as a stacking fault, grain boundary or twin boundary [17] but only the stacking fault is consistent with all the observations. (In a grain boundary or twin boundary, for example, the lattice orientations on either side of the boundary differ, whereas a stacking fault is a planar defect where, within a single atomic (or molecular) layer, although the stacking sequence of the layers is changed, this does not result in a change in the orientation of the lattice.) It must be concluded therefore that the defects seen in Figs 5 and 6 are stacking faults.

The displacement vector, **R**, of a stacking fault can be found by determining the extinction conditions for the fault when it is observed in dark-field using different **g**-vectors. Using this technique **R** can be determined from the criterion [17] that for the fault to be invisible the product of the reciprocal lattice vector of the spot used to image the fault and **R**, the displacement vector, must have an integral value (including zero), i.e. $\mathbf{g}\cdot\mathbf{R}$ = integer. The stacking fault will be visible when $\mathbf{g}\cdot\mathbf{R}$ takes non-integral values. Dark-field micrographs of the same area of a crystal taken using different **g**-vectors are given in Fig. 6 and it can be seen that the contrast from the stacking faults is in some cases weak and in other cases strong. Similar observations have been made for many stacking faults in different pTS crystals and the results are summarized in Table I. A displacement vector **R** consistent with all the experimental

TABLE I Contrast observed from stacking faults in pTS crystals observed in different dark-field conditions. Values of $\mathbf{g}\cdot\mathbf{R}$ are given for $\mathbf{R} = \frac{1}{2}[1\,\bar{2}\,1]$

g	Contrast	g·R
$2\,\bar{1}\,1$	s	5/2
$2\,\bar{1}\,\bar{1}$	s	3/2
$2\,\bar{1}\,0$	w	2
$4\,\bar{2}\,1$	s	9/2
0 0 2	w	1
$1\,0\,\bar{1}$	w	0
$2\,\bar{1}\,2$	w	3

s = strong
w = weak

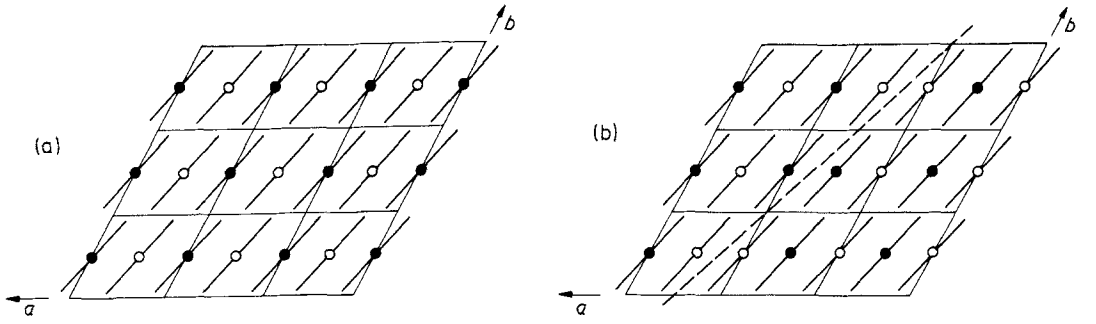

Figure 7 Schematic sketch of 9 unit cells of a pTS crystal viewed parallel to the chain direction. (a) Perfect crystal; (b) crystal containing a stacking fault, indicated by the broken line.

observations is $\mathbf{R} = \frac{1}{2}[1\,\bar{2}\,1]$ and the product $\mathbf{g}\cdot\mathbf{R}$ is also given in Table I. It can be seen that the product has integral values when the contrast is weak and non-integral values when the contrast is strong. No other value of $\mathbf{R}$ was found which gave similar agreement.

4.2. Stacking fault and molecular structure

It is of interest to examine what is meant by a stacking fault with a displacement vector of $\mathbf{R} = \frac{1}{2}[1\,\bar{2}\,1]$ in terms of the perturbation produced in the molecular stacking. The plane of the stacking fault can be calculated from the line of the fault and the displacement vector, $\mathbf{R}$. The plane of the fault must contain both the line, [0 0 1] and $\mathbf{R}$, $[1\,\bar{2}\,1]$: the only plane which can contain these two directions is (2 1 0). The crystal structure of pTS [14, 15] is represented schematically in Fig. 7a as a projection parallel to the chain axis. There are two molecular segments per unit cell and the molecules tend to be planar with the side groups lying approximately in the (2 1 0) planes. The same crystal structure containing the stacking fault identified above is sketched in Fig. 7b. The displacement vector can be thought of as being made up of two components,

$$\mathbf{R} = \tfrac{1}{2}[1\,\bar{2}\,1] \equiv \tfrac{1}{2}[1\,\bar{2}\,0] + \tfrac{1}{2}[0\,0\,1], \quad (1)$$

which are a displacment of one layer of molecules in a (2 1 0) plane by $\frac{1}{2}[1\,\bar{2}\,0]$ perpendicular to the chain direction followed by the same layer being displaced by $c/2$ in the chain direction. Only the displacement of $\frac{1}{2}[1\,\bar{2}\,0]$ is seen in the projection in Fig. 7b.

A question arises as to the likelihood of such a stacking fault occurring, in terms of the molecular structure and the experimental observations. The stacking-fault can be produced by a simple displacement of one layer of molecules on a (2 1 0) plane. This would seem to be very reasonable as the side groups of the molecules lie in the (2 1 0) planes and so the displacement required for the stacking fault does not disrupt either the molecular back-bone or the relatively large side-groups. Clearly a simple displacement of $\frac{1}{2}[1\,\bar{2}\,0]$ would cause problems because this displacement puts a layer of molecules into the incorrect positions in the crystal structure. The two types of molecule in each unit cell are related to each other by a diad screw axis [14]. It appears that a further displacement of $\frac{1}{2}[0\,0\,1]$ is required in order to relieve the packing.

The stacking fault is seen in the pTS crystals in the electron microscope as a band of finite and variable width lying parallel to the chain direction. This is consistent with the defect being due to a fault in the stacking of the (2 1 0) planes. These planes lie at an angle of 42° to the (0 1 0) crystal surface which will cause the stacking fault to project as a band parallel to the chain direction. Also, in the wedge-shaped crystal in Fig. 5 the stacking fault would be expected to taper towards the edge. In addition, knowledge of the plane on which the stacking-fault lies allows the thickness of the crystals to be estimated: The crystal in Fig. 5 thickens from about 130 nm at the edge to over 500 nm in the centre; the crystal in Fig. 6 is approximately 100 nm thick. This could be a useful method of determining the crystal thickness as other methods require knowledge of the extinction distance ξ_g [17] which is very difficult to calculate for the pTS crystal since the structure is monoclinic and there are a large number of atoms in the unit cell. In fact, it may be possible to calculate ξ_g from the spacing of the fringes within the stacking fault (see p. 230 of [17]).

5. Stacking faults in polymer crystals

Stacking faults can be formed in crystals in two ways: the may occur during crystal growth or they

can be formed by the motion of partial dislocations during deformation. In both cases the defects will only form if the stacking-fault energy is sufficiently low. Although it has been proposed that stacking faults may be present in polymer crystals [20], this is the first example of the direct observation of such defects. Recently, Petermann and Gohil [21] found contrast in lamellar crystals of polyethylene and isotatic polyethylene which they interpreted as being probably due to the presence of screw dislocations although they pointed out that similar contrast could also be found if the crystals contained stacking faults.

Having now observed and identified stacking faults in pTS crystals it is of interest to look at the general characteristics of such defects.

(a) Stacking faults lie in planes containing the chain direction, e.g. in the (h k 0) planes when c is the chain direction. This means that the fault does not deform or strain the molecular back-bone. It is also consistent with a prediction of Wunderlich [20] of stacking faults in polyethylene. He suggested that a likely stacking fault would comprise a layer of monoclinic stacking between planes of orthorhombic stacking, which again does not effect the molecular back-bone.

(b) Dislocations must be present where the stacking faults terminate within the crystal. This is clear from Fig. 6 where an array of dislocations can be seen where the stacking faults terminate and similar arrangements are also found in metal crystals [17]. Normally the stacking faults terminate at the edge of the crystal, as can be clearly seen in Fig. 5.

(c) A greater density of stacking faults can be produced by growing the crystals more rapidly. It was found that more stacking faults were produced by allowing the solvent to evaporate in an air-flow rather than allowing evaporation to take place in still air where crystal growth would be slower.

An important question arises from the observation of stacking faults in the pTS crystals as to whether or not the stacking faults are formed in the monomer crystals either during growth or following deformation or if they form during polymerization. This is rather difficult to decide using electron microscopy since the monomer crystals polymerize rapidly on exposure to the electron beam. However, it seems likely that the stacking faults are inherent defects present in the monomer crystals since polymerization takes place through a rearrangement in bonding without any phase change or diffusion [6].

Acknowledgements

The authors are grateful to Dr D. Bloor for supplying the monomer crystals. Financial support from the Science Research Council, The Deutsche Forschungsgemeinschaft and the Alaxander von Humboldt Stiftung is gratefully acknowledged. The authors would like to thank Dr D. Bloor and Professor H. Gleiter for helpful discussions and RJY is grateful to Queen Mary College for granting him study leave in Germany.

References

1. A. KELLER, *Rep. Prog. Phys.* **31** (1968) 623.
2. D. T. GRUBB, *J. Mater. Sci.* **9** (1974) 1715.
3. P. H. LINDENMEYER, *J. Polymer Sci. C* **15** (1966) 109.
4. V. F. HOLLAND and P. H. LINDENMEYER, *J. Appl. Phys.* **36** (1965) 3049.
5. J. PETERMANN and H. GLEITER, *Phil. Mag.* **25** (1972) 813.
6. G. WEGNER, *Pure and Appl. Chem.* **49** (1977) 443.
7. R. H. BAUGHMAN, R. R. CHANCE and M. J. COHEN, *J. Chem. Phys.* **64** (1976) 1869.
8. G. WEGNER, *Z. Naturforsch* **24b** (1969) 824.
9. J. PETERMANN and J. M. SCHULTZ, *J. Mater. Sci.* **14** (1979) 891.
10. J. M. SCHULTZ and J. PETERMANN, *Phil. Mag.* **A40** (1979) 27.
11. R. T. READ and R. J. YOUNG, *J. Mater. Sci.* **14** (1979) 1968.
12. R. J. YOUNG, R. T. READ, D. BLOOR and D. J. ANDO, Faraday Discussion **68** (1979) 510.
13. W. SCHERMANN, G. WEGNER, J. O. WILLIAMS and J. M. THOMAS, *J. Polymer Sci. Polymer Phys. Ed.* **13** (1975) 753.
14. D. KOBELT and E. F. PAULUS, *Acta Cryst.* **B30** (1974) 232.
15. D. BLOOR, L. KOSKI, G. C. STEVENS, F. H. PRESTON and D. J. ANDO, *J. Mater. Sci.* **10** (1975) 1678.
16. W. JONES and J. M. THOMAS, *Prog. Sol. Stat. Chem.* **12** (1979) 1678.
17. P. B. HIRSCH, A. HOWIE, R. B. NICHOLSON, D. W. PASHLEY and M. J. WHELAN, "Electron Microscopy of Thin Crystals" (Butterworths, London, 1965).
18. B. F. BUXTON, J. A. EADES, J. W. STEEDS and G. M. RACKHAM, *Proc. Roy. Soc.* **A281** (1976) 15.
19. M. D. SHANNON and J. A. EADES, *Phil. Mag.* **A40** (1979) 125.
20. B. WUNDERLICH, "Macromolecular Physics: Crystal Structure, Morphology, Defects" (Academic Press, New York and London, 1973).
21. J. PETERMANN and R. M. GOHIL, *Polymer* **20** (1979) 596.

Received 13 November 1980 and accepted 18 February 1981.